Fabrication of Uniform Graphene Discs *via* Transversal Cutting of Carbon Nanofibers

Donghui Long,[†,⊥] Jin-Yong Hong,[‡,⊥] Wei Li,[†] Jin Miyawaki,[†] Licheng Ling,[§] Isao Mochida,[†] Seong-Ho Yoon,[†,*] and Jyongsik Jang[‡,*]

[†]Institute for Materials Chemistry and Engineering, Kyushu University, Kasuga, Fukuoka 816-8580, Japan, [‡]World Class University (WCU) Program of Chemical Convergence for Energy & Environment (C_2E_2), School of Chemical and Biological Engineering, Seoul National University, 599 Gwanangro, Gwanak-gu, Seoul 151-742, Korea, and [§]State Key Laboratory of Chemical Engineering, East China University of Science and Technology, Shanghai 200237, China. [⊥]These authors contributed equally to this work.

ABSTRACT The graphene discs with well-defined shape are successfully fabricated using a simple oxidation and exfoliation process of high-crystalline carbon nanofibers (CNFs). To control the shapes of graphene discs, two different types of CNFs (platelet and herringbone-type) are used as starting materials. The CNFs are formed by the perpendicular stacking of graphene discs, resulting in free edges on the external surface and ready access to interlay spaces. Interestingly, the diameter and shape of the graphene discs can be controlled by selectively designing the morphology of starting materials and optimizing the cutting method. In addition, a mechanical reduction method for oxidized graphene discs is also proposed in order to combine the high recovery of π-conjugated electronic structure with the solution processability of graphene discs. The reduced graphene discs can be formed without any additives, such as reducing agent, and are highly dispersed in different solvents with a high content of graphene discs. This novel strategy offers great possibility for fabricating various graphene-based nanomaterials with rational nanostructure design.

KEYWORDS: carbon nanofiber · graphene · nanomaterials · mechanical reduction · shape control

Graphene, a single layer of carbon atoms arranged in a 2D hexagonal lattice, is a basic building block for graphitic materials of all other dimensionalities.[1−4] It can be wrapped up into fullerene (0D), rolled into carbon nanotube (1D), or stacked into graphite (3D). The graphene exhibits many fascinating properties such as quantum Hall effect, an ambipolar electric field effect, extremely high charge carrier mobility, thermal conductivity, and chemical and mechanical stability. Therefore, graphene is emerging to be a valuable platform for a wide range of applications, including energy storage materials, electronic devices, polymer composites, liquid crystal devices, and bio- and chemical sensors.[5−15]

Up to date, diverse synthetic strategies for preparing graphene have been developed. The most straightforward way to fabricate graphene is the exfoliation method to "peel-off" from graphite. In addition, the graphene can be formed by physical and chemical synthetic techniques, including chemical vapor deposition (CVD) and arc discharge, epitaxial growth, thermal decomposition of SiC, and so forth.[16−22] Recently, multiwalled carbon nanotubes (MWCNTs) have been longitudinally unzipped through chemical exfoliation or plasma etching to obtain graphene with ribbon structure.[23,24] However, most previous synthetic methods suffer from the precise control of the size, shape, edge, and layer of graphene. Therefore, it is still challenging to produce graphene with tailored morphology and diameters for various applications.

In general, the graphene cannot be readily dispersed in water or other organic solvents and requires the use of surfactants to effectively disperse them. The solution processability of graphene offers fascinating advantages because it is amenable to spin-coating, spray-casting, drop-casting, or inkjet printing onto substrates for large-scale production. The most promising route for solution-processable graphene is the oxidation and subsequent exfoliation of graphite in the liquid phase due to hydrophilicity of graphene oxide. In this case, graphene oxide should be converted to reduced graphene by chemical reduction and thermal annealing. The reduced graphene forms structural defects and contains residual oxygen-containing groups, which may disrupt the electronic properties of pristine graphene. Therefore, it is also desirable to develop a simple and reliable method to prepare highly concentrated and stable reduced graphene dispersion in various solvents.

Herein, we report a novel route for the fabrication of shape-controlled graphene discs using a simple oxidation and exfoliation process of high-crystalline carbon nanofibers (CNFs). Having demonstrated the feasibility of the above approach, we used two different types of CNFs (platelet and

* Address correspondence to yoon@cm.kyushu-u.ac.jp, jsjang@plaza.snu.ac.kr.

Received for review March 30, 2011 and accepted July 12, 2011.

Published online July 12, 2011
10.1021/nn201195g

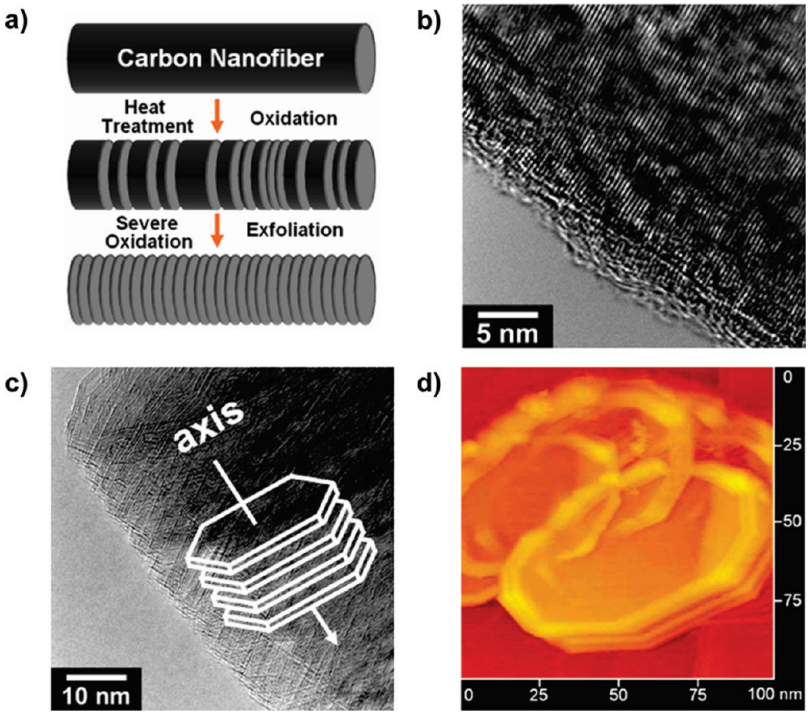

Figure 1. (a) Plausible formation procedure of graphene layers with well-defined shape using the platelet carbon nanofibers. (b) HR-TEM images of as-prepared PCNFs. (c) TEM image of GPCNFs. (d) STM images of isolated graphitized CNFs.

herringbone-type) as starting materials. The diameter and shape of the graphene discs can be controlled by selectively designing the morphology of starting materials and optimizing the cutting method. In addition, a mechanical reduction method for oxidized graphene disc oxide is also proposed to combine the high recovery of π-conjugated electronic structure with the solution processability of graphene discs. Our results demonstrate that the reduced graphene discs can be formed without any additives such as reducing agent and are dispersed in different solvents with high content of graphene discs.

RESULTS AND DISCUSSION

Preparation of Graphitized Carbon Nanofibers. The overall synthetic procedure for graphene discs is represented in Figure 1a. Under our experimental conditions, two different types of high-crystalline CNFs (platelet and herringbone-type) were employed as a starting material. The platelet CNFs (PCNFs) were prepared by the catalytic pyrolysis of carbon monoxide over iron metal particles at 600 °C.[24] The PCNFs had diameters of 80−300 nm with a polygonal cross section according to SEM observation (Supporting Information, Figure S1), and the PCNFs had very high carbon content with the elemental composition of C (99.0%), H (0.2%), and O (0.8%). XRD pattern revealed that the PCNFs had a high degree of graphitization with the interlayer distance (d_{002}) of *ca.* 0.336 nm, comparable to those of natural graphite. However, the high-resolution TEM image (Figure 1b) displays that the graphitic interlayer is not strictly straight and some dislocation and tortuosity exist in the local region.

To improve the crystalline phase of graphite structure, the pristine PCNFs were further graphitized in argon atmosphere at 2800 °C. The graphitized PCNFs (GPCNFs) had similar XRD pattern of crystal structure but different microscopic morphologies compared to their pristine PCNFs. As shown in Figure 1c,d and Figures S2 and S3 (Supporting Information), the GPCNFs were constructed by parallel close-packing of nanosized plate units as illustrated in the model of hexagonal-type plate stacking. Such a plate unit had an average thickness of *ca.* 3 nm consisting of 8−10 graphene discs. This stacking formation of the hexagonal-type plate was due to rearrangement and reorganization in the postgraphitization. In addition, it also inherited the primal embryo in the as-prepared PCNFs as a reflection of the periodical repetition of temporal nucleation and growth of graphene layers.[25,26]

Oxidation and Exfoliation of Graphitized Carbon Nanofibers. After postgraphitization, the GPCNFs were suspended in concentrated sulfuric acid followed by $KMnO_4$ treatment according to the Hummer's method.[27] Figure 2 demonstrates that the TEM image of oxidized GPCNFs is a function of mass ratio of oxidant to GPCNFs ($KMnO_4$/GPCNF, $R_{K/GP}$). After the oxidation process, the oxidized GPCNFs were exfoliated under ultrasonic assistance for 1 h. The oxidized graphene discs were readily exfoliated from the oxidized GPCNFs. It was found that 1 h ultrasonic treatment is enough to achieve complete exfoliation of oxidized GPCNFs to the individual oxidized graphene

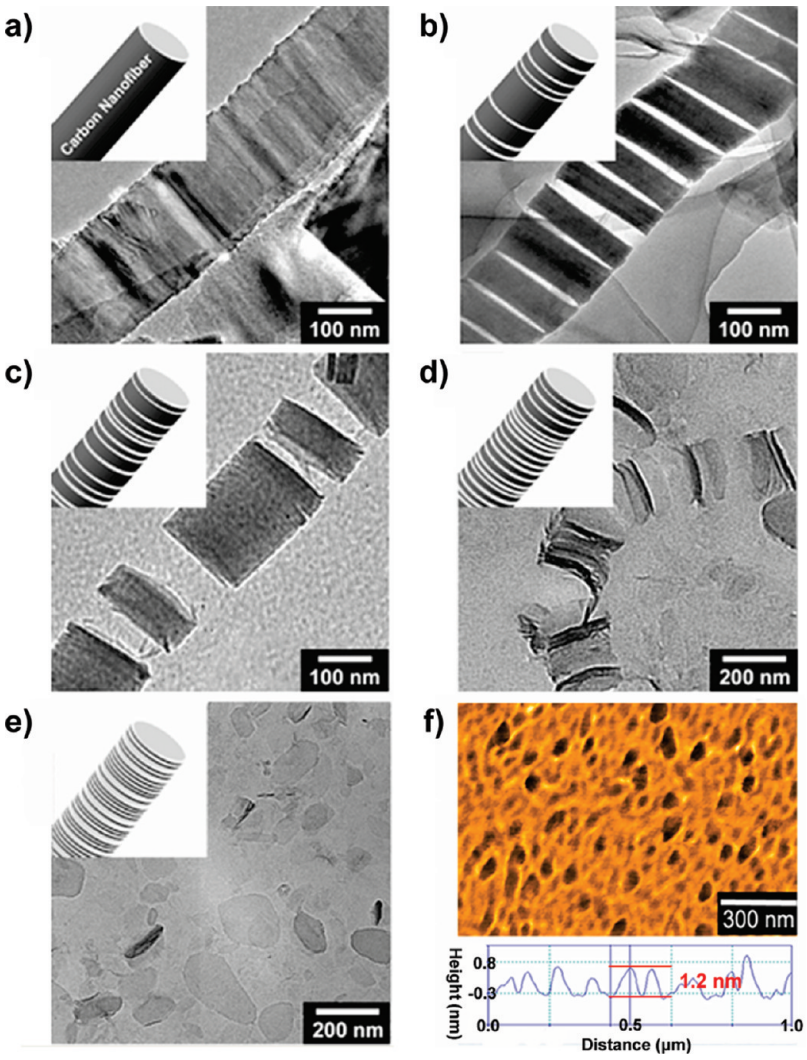

Figure 2. TEM images (a−e) for oxidized GPCNFs as a function of mass ratio of oxidant to GPCNFs: (a) pristine GPCNFs, (b) $R_{K/GP}$ = 1, (c) $R_{K/GP}$ = 2, (d) $R_{K/GP}$ = 3, (e) $R_{K/GP}$ = 6 (inset, related schematic illustration), (f) AFM image of exfoliated oxidized graphene discs with the mean thickness of 1.2 nm.

discs. A high degree of exfoliation was observed as the oxidation level increased in the range of 1−6 ($R_{K/GP}$).

In the case of the $R_{K/GP}$ of 1, the GPCNFs still maintained their integrity even though many kerfs were homogeneously distributed (Figure 2b). When the $R_{K/GP}$ value increases to 2, the oxidized GPCNFs broke into small segments and still contained tens of plate units. These segments could be further split into smaller ones up to an $R_{K/GP}$ value of 3. Further increasing the $R_{K/GP}$ value to 5, most of the plate units were isolated and some oxidized graphene discs were separated from the structure units (Supporting Information, Figure S4). Increasing the $R_{K/GP}$ value to 6, we obtained high quality and uniform oxidized graphene discs with average thickness of 1.2 nm. This phenomenon demonstrated that the single-layered oxidized graphene discs were successfully exfoliated from the GPCNFs. However, perfectly thin graphene discs could not be obtained up to the $R_{K/GP}$ value of 7−10, due to structural collapse of GPCNFs based on the excessive oxidation.

The structure evolution from GPCNFs to oxidized GPCNFs was investigated with different oxidation levels by XRD analysis (Figure 3a). The treated samples at an $R_{K/GP}$ value of 1 and 2 had a relatively broad peak at 2θ values of ~26° (a d_{002} spacing of 3.37 nm), originating from the graphitic structure. In the case of $R_{K/GP}$ value of 3−6, this peak dramatically diminished but a new shape peak appeared at ~10.5° (d-spacing value of 0.76 nm), which was very similar to that of graphitic oxide.[28]

In addition, the GPCNFs with different oxidation levels were analyzed by elemental analysis (EA), XPS, and solid ^{13}C NMR. As shown in Table S1 (Supporting Information), the C/O/H ratio of oxidized GPCNFs varied from 6.00:0.50:0.56 ($R_{K/GP}$ = 1) of initial oxidation level to 6.00:2.89:4.48 of high oxidation level ($R_{K/GP}$ = 6). From the XPS spectra of oxidized GPCNFs (Supporting Information, Figure S5), deconvolution of the C 1s spectra showed five individual component groups that represented graphitic carbon (C_{G1}, 284.4 eV) and carbon present in phenol, alcohol, or ether (C_{G2}, 286.1 ± 0.3 eV), carbonyl or quinine

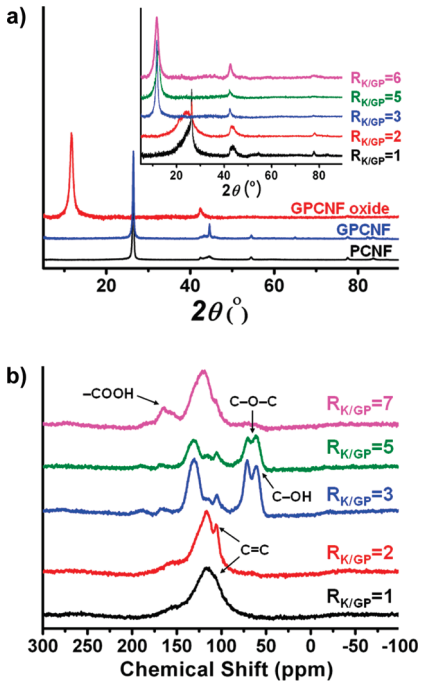

Figure 3. (a) XRD patterns of platelet CNF, graphitized platelet CNFs (GPCNFs), and oxidized GPCNFs (inset, changes in XRD patterns of GPCNFs as a function of $R_{K/GP}$ value). (b) Solid ^{13}C NMR of oxidized GPCNFs with a different $R_{K/GP}$ value.

groups (C_{G3}, 287.3 ± 0.3 eV), carboxyl, lactone, or ester groups (C_{G4}, 289.1 eV), and carbonate groups (C_{G5}, 290.6 eV). Deconvolution of the O 1s spectra yielded four peaks; the peak at 531.0−531.3 eV (O_{G1}) corresponded to carbonyl oxygen atoms; the peak at 532.1−532.5 eV (O_{G2}) corresponded to carbonyl oxygen atoms in esters, amides, and anhydrides as well as oxygen atoms in hydroxyls or ethers; the peak at 533.1−533.5 eV (O_{G3}) corresponded to ether oxygen atoms in esters and anhydrides; and the peak at 534.1−534.4 eV (O_{G4}) corresponded to oxygen atoms in carboxyl groups. Consequently, the XPS spectra reveal that the oxidized GPCNFs consisted mainly of carbonyl, carboxyl and hydroxyl groups. The solid-state ^{13}C NMR spectra of GPCNFs at $R_{K/GP}$ = 3−6 (Figure 3b) showed C−OH, C−O−C epoxide, conjugated double groups, aromatic entities, and carboxylic groups at 60, 70, 105, 130, and 165 ppm, respectively, which might be the same as the structure of graphite oxide.[29,30] As determined from these data, it is concluded that the oxidized GPCNFs are generated by oxidation using $KMnO_4$ as am oxidizing agent and contain a wide range of oxygen functional groups, such as hydroxyl and epoxy groups on the basal plane and carboxylic acid groups at the edges, which make the GPCNFs hydrophilic. The oxygen functional groups in the GPNCFs allow dynamic intercalation of water molecules into the GPCNFs. Furthermore, the interlayer distance is also directly connected to dispersity of aqueous oxidized GPCNF solution. That means that the water molecules are highly bound to the oxidized graphene discs. Then the dispersity and stability can be enhanced. Consequently, the high $R_{K/GP}$ value ($R_{K/GP} \approx 6$) enables one to achieve complete exfoliation and obtain high quality and uniform oxidized graphene discs.

Interestingly, the diameter of graphene discs was in accordance with that of the PCNFs, which could be controlled by changing the chemical vapor decomposition conditions of the CNF growth process. The PCNFs with small diameters of 30−50 nm could be prepared from carbon monoxide over a Fe/Co/Ni/MgO (7.0:2.0:0.5:0.5 in weight ratio) catalyst at 600 °C, allowing the fabrication of graphene discs with small diameter (Figure 4).

Except the PCNFs, the herringbone type of CNFs (HCNFs) was also used as a starting material. Figure 5 illustrates the graphitized HCNFs and oxidized graphitized HCNFs with different morphology. The HCNFs with diameters ranging from 150 to 200 nm were prepared from carbon monoxide over Fe/Mn (3:7) alloy catalyst at 560 °C. As a consequence or their high crystallinity and different morphology, the HCNFs also readily oxidized and exfoliated, which cause the bow-tie shape of graphene discs (Figure 5b inset). It was noteworthy that the graphene discs with different defined shapes could be obtained by selectively designing the shape of starting materials and optimizing the transversal cutting method.

Mechanical Reduction of Oxidized Graphene Discs. Since the discovery of graphene in 2004, there have been numerous research papers published that have demonstrated the various reduction processes for graphene oxide. Surveys of the main results obtained in this field have been summarized in several papers.[31,32] In this work, we report an alternative reduction method based on green technology (GT). A mechanical reduction method for graphene oxide is also proposed to combine the high recovery of π-conjugated electronic structure with the solution processability of graphene discs. First, the oxidized graphene discs were oxidized and then completely exfoliated from graphitized carbon nanofibers (GPCNFs). Reduction of oxidized graphene discs containing oxygen functional groups can be explained by dehydration of oxidized graphene discs in acidic aqueous medium as a source of H^+ (Supporting Information, Scheme S1). The mechanical reduction based on a wet milling technology also can be considered. Oxidized graphene disc solution was put into the chamber with a Filmics mixer that created a centrifugal field of *ca.* 18 400 rpm. This high-speed revolution of turbine caused the oxidized graphene discs to collide with each other and endowed high surface energy to reduce the oxygen-containing functional groups and formed the sp^2 structure of carbon without any additives such as reducing agent.

Figure 6 depicts UV−vis absorption spectra of reduced graphene discs. The reduction time directly affects the reduction of a colloidal suspension of exfoliated graphene discs. The oxidized graphene discs had a maximum absorption wavelength (λ_{max}) at 230 nm related to $\pi-\pi^*$ electron transition in the

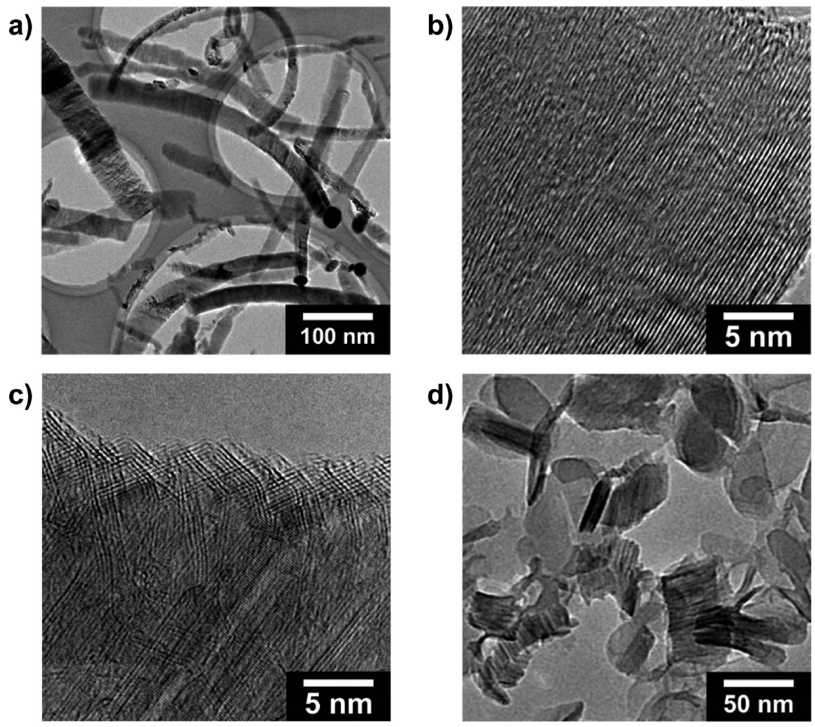

Figure 4. TEM images of as-prepared (a,b) and graphitized platelet carbon nanofibers (c). The platelet carbon nanofibers has a relatively small diameter of *ca.* 30−50 nm, allowing the fabrication of small diameter graphene discs (d). Graphene discs are oxidized under controlled conditions ($R_{K/GP}$ = 3) and reduced by using a mechanical reduction method.

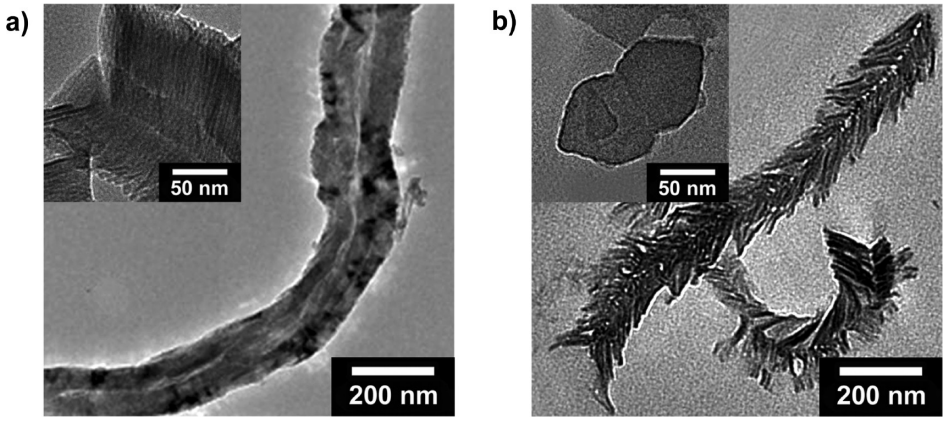

Figure 5. TEM images of (a) graphitized herringbone carbon nanofibers and (b) oxidized graphitized herringbone carbon nanofibers ($R_{K/GP}$ = 3) (inset, isolated bow-tie-shaped graphene discs).

polyene-type structure. However, the reduced graphene discs (at 50 min of reduction time) exhibited a λ_{max} at 268 nm, which was contributed by $\pi-\pi^*$ electron transition in the polyaromatic system. In a mechanical reduction process, both the bathochromic shift of λ_{max} and the hyperchromicity were observered in the entire range (>230 nm). These phenomena indicated that the π-conjugated electronic structure of graphene discs could be gradually recovered with increasing reduction time.[23]

Figure 7 also demonstrates the Raman spectra of as-prepared samples under various reaction procedures. The Raman I_D/I_G ratio is widely used to evaluate the quality of graphene nanomaterials. In general, I_D/I_G ratio of graphene is related to density of defects, as well as edge smoothness and edge structures (that is, arm-chair and zigzag). However, because the edge structures of the graphene discs are unknown as yet, the I_D/I_G average ratio may reflect the quality of the graphene discs (including edge roughness, defects). Under our experimental conditions, all prepared samples represented a weak and broad band from 1250 to 3500 cm^{-1}. The Raman spectra indicated two strong wide bands near 1582 and 1357 cm^{-1}. The peak located near 1582 cm^{-1} is due to the graphitic structure, whereas the peak near 1357 cm^{-1} originates from disordered structure in the carbon. The Raman spectrum of the pristine GPCNFs, as expected, displays a

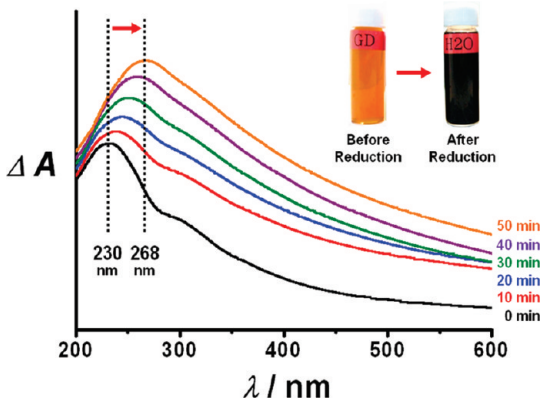

Figure 6. UV−vis absorption spectra of reduced graphene disc solution as a function of reduction time.

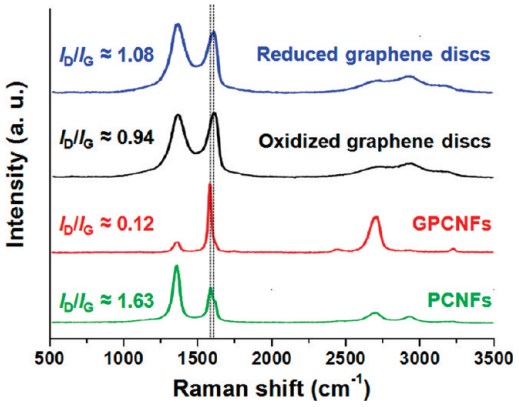

Figure 7. Raman spectra of reduced graphene discs, oxidized graphene discs, GPCNFs, and PCNFs. Graphene discs are oxidized under controlled conditions ($R_{K/GP}$ = 6) and reduced by using a mechanical reduction method.

prominent G peak, corresponding to the first-order scattering of the E2g mode ($I_D/I_G \approx 0.12$). In the Raman spectrum of oxidized graphene discs, the G band is broadened and shifted to 1594 cm^{-1}. In addition, the D band at 1363 cm^{-1} becomes prominent, indicating the reduction in size of the in-plane sp^2 domains, possibly due to the extensive oxidation. The Raman spectrum of the reduced graphene discs also contains both G and D bands, however, with an increased D/G intensity ratio ($I_D/I_G \approx 1.08$) compared to that of oxidized graphene discs ($I_D/I_G \approx 0.94$). This change suggests that the oxidized graphene discs are transformed from amorphized states to more graphitic structures with significant amounts of defects.[33,34]

To provide evidence that the reduction time affects the degree of reduction directly, the reduced graphene discs were also investigated by XRD, solid ^{13}C NMR, elemental analysis, XPS techniques, Fourier transform infrared spectrometry (FT-IR), atomic force microscopy (AFM), and four-probe conductivity measurement (see Supporting Information, Figures S6, S7, S8, S9, and S10 and Table S2). Taking these results into account, we conclude that both the acid-catalyzed dehydration and

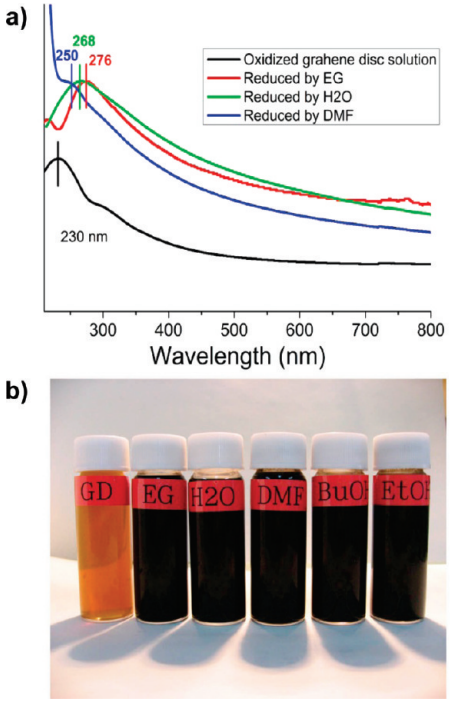

Figure 8. UV−vis absorption spectra of oxidized graphene disc solution (a) and resultant graphene disc solution reduced by water, ethylene glycol, *N*,*N*-dimethyl formamide, *n*-butanol, and ethanol (b). Graphene disc solution is oxidized under controlled conditions ($R_{K/GP}$ = 6) and reduced by using a mechanical reduction method.

the high surface energy caused by wet milling technology give a combined or synergistic contribution to reduction of oxidized graphene discs into reduced graphene discs. The oxygen-containing functional groups were significantly removed from the surface of graphene discs as the mechanical reduction process proceeded gradually. The mechanical reduction of graphene discs can also be performed using other solvents such as ethylene glycol, propanol, and *N*,*N*-dimethyl formamide. UV−vis absorption spectra also showed that the ethylene glycol provided best reduction performance owing to its intrinsic reduced characteristics (Figure 8a). After the mechanical reduction, all prepared solutions exhibit a change of color from brown yellow to black and, notably, still kept in stable solution state. It could be ascribed in terms of the mixing effect, which prevented secondary agglomeration of graphene discs during the mechanical reduction process. By employing this mechanical reduction, we could prepare graphene disc solution with a concentration over 2.0 g/L (Figure 8b).

CONCLUSION

In conclusion, the graphene discs with well-defined shape are successfully fabricated using a simple oxidation and exfoliation process of high-crystalline CNFs. To control the shapes of graphene, two different types of CNFs (platelet and herringbone-type) are used as starting materials. Interestingly, the diameter and shape of the graphene discs can be controlled by selectively designing

the morphology of starting materials and optimizing the cutting method. Furthermore, a mechanical reduction method for graphene oxide is also proposed in order to combine the high recovery of π-conjugated electronic structure with the solution processability of graphene discs. The reduced graphene discs can be formed without any additives such as reducing agent and are highly dispersed in different solvents with high content of graphene discs. Importantly, the developed methodology may provide a convenient way for fabricating novel nanostructured carbon materials with controlled shape and diameter.

MATERIALS AND METHODS

Preparation of Graphitized CNFs. Platelet CNFs were synthesized from carbon monoxide and hydrogen (160/40 v/v, mL/min) over an Fe catalyst at 600 °C. The herringbone CNFs with diameters ranging from 150 to 200 nm were prepared from carbon monoxide over Fe/Mn (3:7) alloy catalyst at 560 °C. The two different types of CNFs were purified in the 10 wt % HCl until the metal content was less than 0.2 wt %. These purified CNFs were further heat-treated at 2800 °C for 10 min to obtain graphitized CNFs.

Oxidation and Exfoliation of Graphitized CNFs. The graphitized CNFs were oxidized according to the Hummer's method. In a typical process, 1 g of graphitized CNFs was suspended in 100 mL of concentrated sulfuric acid with the assistance of 30 min ultrasonication (ultrasonic bath cleaner USK-4R). Then, 1−7 g of potassium permanganate ($KMnO_4$) was slowly added into the solution. The reaction mixture was stirred at 0 °C for 30 min and then heated to 40 °C for an additional 1 h. After that, 100 mL of distilled water was added slowly into the solution within the ice water bath. While the temperature cooled to room temperature (about 2 h), 400 mL of distilled water and 20 mL of 30 wt % H_2O_2 were added. The obtained solution was separated using a centrifuge (Hitachi, Himac CR-GII) at the speed of 4800 rpm, and the remaining slurry was washed with 3 M HCl three times and acetone five times using the centrifuge. The collected samples were dried using freeze-drying equipment (EVELA, FD-1000). After oxidation/washing process, the oxidized graphitized CNFs were exfoliated under ultrasonic assistance for 1 h. The concentration of oxidized graphitized CNFs solution is 2.0 g/L.

Mechanical Reduction of Oxidized Graphene Discs. The reduction was dependent upon a wet milling technology using a nanodispersion machine (T.K.FILMICS 56, PRIMIX) without any assistance of reduced agent. About 70 mL of oxidized graphene disc solution (2.0 g/L) was put into the chamber with a Filmics mixer. The motor was set as 200 V, 3.7 kW, and mixing section rpm was *ca.* 18 400 rpm. The temperature of the solution was controlled by cooling agents to maintain the water temperature around 100 °C. The mixing time was changed from 10 to 50 min.

Characterization. X-ray diffraction was performed with Rigaku X-ray diffractometer with CuK target. High-resolution solid-state ^{13}C NMR experiments were carried out on a JEOL ECA400 spectrometer operated at 100.53 MHz using the single pulse decoupling method. The elemental composition was obtained from the CHN elemental analysis (Yanako MT2 CHN Corder, Japan). X-ray photoelectron spectroscopy (XPS) spectra were obtained using a JPS-9000MC (JEOL) instrument equipped with an Mg K X-ray source. Field emission (FE) tests were performed in a vacuum chamber at a pressure of 7×10^{-8} Pa. Prior to elemental analysis and XPS measurement, samples were dried for 2 h at 120 °C. The UV−vis adsorption spectra were recorded under a Shimadzu UV-3600 spectrophotometer. The morphology of sample was observed under a field-emission scanning electron microscope (JEOL-6300F, JEOL, Japan), a high-resolution transmission electron microscope (JEM-2010F, JEOL, Japan), and an atomic force microscope (Nanoscope IIIa, Digital Instrument, USA). AFM topography analysis was carried out with a Digital Instruments Nanoscope IIIA from Veeco Systems in tapping mode using silicon tips with a resonance frequency of 320 kHz. Raman spectra were recorded using a Bruker FRA 106/S FT-Raman spectrometer with 1064 nm laser excitation (a spectral resolution of 1 cm^{-1}). The peak positions obtained from the Raman spectrometer have a margin of error of ± 0.05 cm^{-1}. For Raman spectroscopy analysis, the samples were dried in a vacuum oven for 12 h at room temperature and were examined under ambient conditions without any pretreatment.

Acknowledgment. This work was supported by the National Research Foundation of Korea (NRF) grant funded by the Korea government (MEST) (No. 2011-0017125) and the WCU (World Class University) program through the National Research Foundation of Korea funded by the Ministry of Education, Science and Technology (R31-10013) and the Management Expenses Grants for National Universities Corporations from the Ministry of Education, Culture, Sports, Science and Technology of Japan (MEXT), and GCOE (NCRS) in Kyushu University.

Supporting Information Available: (1) SEM images of as-prepared and graphitized platelet carbon nanofibers, (2) TEM images of as-prepared and graphitized platelet carbon nanofibers, (3) STM images of graphitized PCNFs, (4) TEM images of isolated GPCNFs, (5) elemental and physical parameter of oxidized GPCNFs, (6) XPS spectra of oxidized GPCNFs, (7) de/hydration mechanism of oxidized graphene discs, (8) XRD patterns of graphene discs, (9) solid ^{13}C NMR spectra of graphene discs, (10) XPS C1s spectra of graphene discs, (11) Fourier transform infrared spectrometry (FT-IR) of graphene discs, (12) atomic force microscope (AFM) analysis of graphene discs, (13) and electrical properties of graphene discs. This material is available free of charge *via* the Internet at http://pubs.acs.org.

REFERENCES AND NOTES

1. Geim, A. K.; Novoselov, K. S. The Rise of Graphene. *Nat. Mater.* **2007**, *6*, 183–191.
2. Guinea, F.; Katsnelson, M. I.; Geim, A. K. Energy Gaps and a Zero-Field Quantum Hall Effect in Graphene by Strain Engineering. *Nat. Phys.* **2010**, *6*, 30–33.
3. Wassei, J. K.; Kaner, R. B. Graphene, A Promising Transparent Conductor. *Mater. Today* **2010**, *13*, 52–59.
4. Becerril, H. A.; Mao, J.; Liu, Z.; Stoltenberg, R. M.; Bao, Z.; Chen, Y. Evaluation of Solution-Processed Reduced Graphene Oxide Films as Transparent Conductors. *ACS Nano* **2008**, *2*, 463–470.
5. Liao, K. H.; Mittal, A.; Bose, S.; Leighton, C.; Mkhoyan, K. A.; Macosko, C. W. Aqueous Only Route toward Graphene from Graphite Oxide. *ACS Nano* **2011**, *5*, 1253–1258.
6. Lotya, M.; King, P. J.; Khan, U.; De, S.; Coleman, J. N. High-Concentration, Surfactant-Stabilized Graphene Dispersions. *ACS Nano* **2011**, *4*, 3155–3162.
7. Su, C. Y.; Lu, A. Y.; Xu, Y.; Chen, F. R.; Khlobystov, A. N.; Li, L. J. High-Quality Thin Graphene Films from Fast Electrochemical Exfoliation. *ACS Nano* **2011**, *5*, 2332–2339.
8. Park, S.; Ruoff, R. S. Chemical Methods for The Production of Graphenes. *Nat. Nanotechnol.* **2009**, *4*, 217–224.
9. Hong, J.-Y.; Shin, K.-Y.; Kwon, O. S.; Kang, H.; Jang, J. A Strategy for Fabricating Single Layer Graphene Sheets Based on a Layer-by-Layer Self-Assembly. *Chem. Commun.* **2011**, *47*, 7182–7184.
10. Gomez-Navarro, C.; Weitz, R. T.; Bittner, A. M.; Scolari, M.; Mews, A.; Burghard, M.; Kern, K. Electronic Transport Properties of Individual Chemically Reduced Graphene Oxide Sheets. *Nano Lett.* **2009**, *9*, 2206–2206.
11. Marcano, D. C.; Kosynkin, D. V.; Berlin, J. M.; Sinitskii, A.; Sun, Z.; Slesarev, A.; Alemany, L. B.; Lu, W.; Tour, J. M. Improved Synthesis of Graphene Oxide. *ACS Nano* **2010**, *4*, 4806–4814.

12. Luo, J.; Tian, P.; Pan, C. T.; Robertson, A. W.; Warner, J. H.; Hill, E. W.; Briggs, G. A. D. Ultralow Secondary Electron Emission of Graphene. *ACS Nano* **2011**, *5*, 1047–1055.
13. Zhu, Y.; Stoller, M. D.; Cai, W.; Velamakanni, A.; Piner, R. D.; Chen, D.; Ruoff, R. S. Exfoliation of Graphite Oxide in Propylene Carbonate and Thermal Reduction of the Resulting Graphene Oxide Platelets. *ACS Nano* **2010**, *4*, 1227–1233.
14. Wu, Q.; Xu, Y.; Yao, Z.; Liu, A.; Shi, G. Supercapacitors Based on Flexible Graphene/Polyaniline Nanofiber Composite Films. *ACS Nano* **2010**, *4*, 1963–1970.
15. Liu, Z.; Robinson, J. T.; Sun, X.; Dai, H. PEGylated Nanographene Oxide for Delivery of Water-Insoluble Cancer Drugs. *J. Am. Chem. Soc.* **2008**, *130*, 10876–10877.
16. Hernandez, Y.; Nicolosi, V.; Lotya, M.; Blighe, F. M.; Sun, Z.; De, S.; McGovern, I. T.; Holland, B.; Byrne, M.; Gun'Ko, Y. K.; *et al.* High-Yield Production of Graphene by Liquid-Phase Exfoliation of Graphite. *Nat. Nanotechnol.* **2008**, *3*, 563–568.
17. Li, X. L.; Zhang, G. Y.; Bai, X. D.; Sun, X. M.; Wang, X. R.; Wang, E. G.; Dai, H. J. Highly Conducting Graphene Sheets and Langmuir–Blodgett Films. *Nat. Nanotechnol.* **2008**, *3*, 538–542.
18. Berger, C.; Song, Z. M.; Li, T. B.; Li, X. B.; Ogbazghi, A. Y.; Feng, R.; Dai, Z. T.; Marchenkov, A. N.; Conrad, E. H.; First, P. N.; *et al.* Ultrathin Epitaxial Graphite: 2D Electron Gas Properties and a Route toward Graphene-Based Nanoelectronics. *J. Phys. Chem. B* **2004**, *108*, 19912–19916.
19. Emtsev, K. V.; Bostwick, A.; Horn, K.; Jobst, J.; Kellogg, G. L.; Ley, L.; McChesney, J. L.; Ohta, T.; Reshanov, S. A.; R€ohrl, J.; *et al.* Towards Wafer-Size Graphene Layers by Atmospheric Pressure Graphitization of Silicon Carbide. *Nat. Mater.* **2009**, *8*, 203–207.
20. Reina, A.; Jia, X. T.; Ho, J.; Nezich, D.; Son, H.; Bulovic, V.; Dresselhaus, M. S.; Kong, J. Large Area, Few-Layer Graphene Films on Arbitrary Substrates by Chemical Vapor Deposition. *Nano Lett.* **2009**, *9*, 30–35.
21. Li, X. S.; Cai, W. W.; An, J. H.; Kim, S.; Nah, J.; Yang, D. X.; Piner, R.; Velamakanni, A.; Jung, I.; Tutuc, E.; *et al.* Large-Area Synthesis of High-Quality and Uniform Graphene Films on Copper Foils. *Science* **2009**, *324*, 1312–1314.
22. Gao, J. H.; Fujita, D.; Xu, M. S.; Onishi, K.; Miyamoto, S. Unique Synthesis of Few-Layer Graphene Films on Carbon-Doped $Pt_{83}Rh_{17}$ Surface. *ACS Nano* **2010**, *4*, 1026–1032.
23. Kosynkin, D. V.; Higginbotham, A. L.; Sinitskii, A.; Lomeda, J. R.; Dimiev, A.; Price, B. K.; Tour, J. M. Longitudinal Unzipping of Carbon Nanotubes To Form Graphene Nanoribbons. *Nature* **2009**, *458*, 872–876.
24. Jiao, L.; Zhang, L.; Wang, X.; Diankov, G.; Dai, H. Narrow Graphene Nanoribbons from Carbon Nanotubes. *Nature* **2009**, *458*, 877–880.
25. Yoon, S.; Lim, S.; Hong, S.; Qiao, W.; Whitehurst, D. D.; Mochida, I.; An, B.; Yokogawa, K. A Conceptual Model for the Structure of Catalytically Grown Carbon Nano-fibers. *Carbon* **2004**, *43*, 1828–1838.
26. Helveg, S.; Lopez-Cartes, C.; Sehested, J.; Hansen, P. L.; Clausen, B. S.; Rostrup-Nielsen, J. R.; Abild-Pedersen, F.; Norskov, J. S. Atomic-Scale Imaging of Carbon Nanofibre Growth. *Nature* **2004**, *427*, 426–429.
27. Hummers, W. S.; Offeman, R. E. Preparation of Graphitic Oxide. *J. Am. Chem. Soc.* **1958**, *80*, 1339.
28. Bourlinos, A. B.; Gournis, D.; Petridis, D.; Szabo, T.; Szeri, A.; Dekany, I. Graphite Oxide: Chemical Reduction to Graphite and Surface Modification with Primary Aliphatic Amines and Amino Acids. *Langmuir* **2003**, *19*, 6050–6055.
29. He, H. Y.; Riedl, T.; Lerf, A.; Kliowski, J. Solid-State NMR Studies of the Structure of Graphite Oxide. *J. Phys. Chem.* **1996**, *100*, 19954–19958.
30. Lerf, A.; He, H. Y.; Forster, M.; Klinowski, J. Structure of Graphite Oxide Revisited. *J. Phys. Chem. B* **1998**, *102*, 4477–4482.
31. Zhou, Y.; Bao, Q.; Tang, L. A. L.; Zhong, Y.; Loh, K. P. Hydrothermal Dehydration for the "Green" Reduction of Exfoliated Graphene Oxide to Graphene and Demonstration of Tunable Optical Limiting Properties. *Chem. Mater.* **2009**, *21*, 2950–2956.
32. Rourke, J. P.; Pandey, P. A.; Moore, J. J.; Bates, M.; Kinloch, I. A.; Young, R. J.; Wilson, N. R. The Real Graphene Oxide Revealed: Stripping the Oxidative Debris from the Graphene-like Sheets. *Angew. Chem., Int. Ed.* **2011**, *50*, 3173–3177.
33. Su, C. Y.; Xu, Y.; Zhang, W.; Zhao, J.; Tang, X.; Tsai, C. H.; Li, L. J. Electrical and Spectroscopic Characterizations of Ultra-large Reduced Graphene Oxide Monolayers. *Chem. Mater.* **2009**, *21*, 5674–5680.
34. Su, C. Y.; Xu, Y.; Zhang, W.; Zhao, J.; Liu, A.; Tang, X.; Tsai, C. H.; Huang, Y.; Li, L. J. Highly Efficient Restoration of Graphitic Structure in Graphene Oxide Using Alcohol Vapors. *ACS Nano* **2010**, *4*, 5285–5292.